

ReCo-Diff: Explore Retinex-Based Condition Strategy in Diffusion Model for Low-Light Image Enhancement

Yuhui Wu¹, Guoqing Wang¹, Zhiwen Wang¹, Yang Yang¹, Tianyu Li¹, Peng Wang¹,
Chongyi Li², Heng Tao Shen¹

¹University of Electronic Science and Technology of China, ²Nankai University

Abstract

Low-light image enhancement (LLIE) has achieved promising performance by employing conditional diffusion models. Despite the success of some conditional methods, previous methods may neglect the importance of an explicit formulation of task-specific condition strategy, resulting in suboptimal visual outcomes. In this study, we propose ReCo-Diff, a novel approach that incorporates Retinex-based prior as an additional pre-processing condition to regulate the generating capabilities of the diffusion model. ReCo-Diff first leverages a pre-trained decomposition network to produce initial reflectance and illumination maps of the low-light image. Then, an adjustment network is introduced to suppress the noise in the reflectance map and brighten the illumination map, thus forming the learned Retinex-based condition. The condition is integrated into a refinement network, implementing Retinex-based conditional modules that offer sufficient guidance at both feature- and image-levels. By treating Retinex theory as a condition, ReCo-Diff presents a unique perspective for establishing an LLIE-specific diffusion model. Extensive experiments validate the rationality and superiority of our ReCo-Diff approach. The code will be made publicly available.

1. Introduction

Low-light photography is quite prevalent in the real world due to inherent environmental or technology restrictions, such as inadequate lighting and limited exposure times. Images captured in weakly illuminated conditions not only have low visibility for human perception but also are unsuitable for subsequent multimedia computing and downstream vision tasks, such as object detection [3, 19] and semantic segmentation [6]. Therefore, a large number of methods for low-light image enhancement (LLIE) are proposed to expose hidden features in low-light images and avoid performance degradation in subsequent vision tasks.

Thanks to the development of diffusion models (DMs) [13, 33], numerous diffusion-based studies have been conducted for image restoration tasks [28, 31], with the goal of facilitating texture recovery. Previous diffusion-based image restoration methods choose to concatenate the

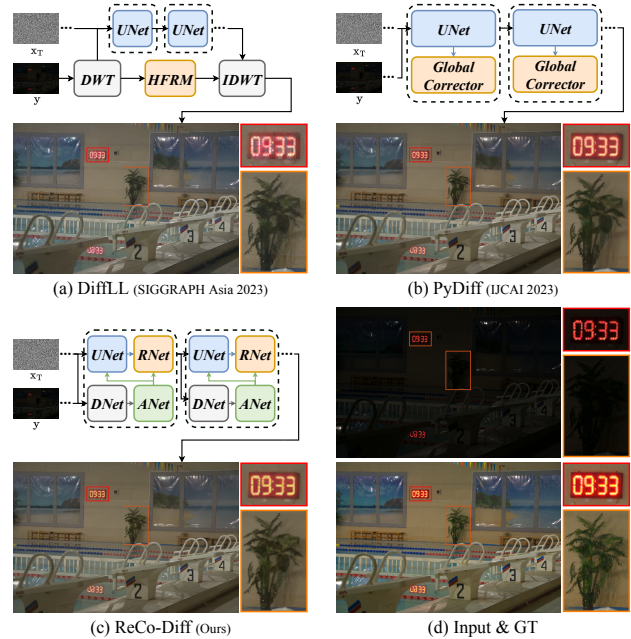


Figure 1. Visual comparisons among recent DiffLL [14], PyDiff [57], and our ReCo-Diff on a low-light image from the LOLv2 dataset. Previous diffusion-based methods exhibit detail loss and color distortion. Our method properly maintains color constancy and generates realistic textures thanks to the introduction of the superior Retinex-based condition strategy.

low/high-quality images [30, 31] and extract features and priors [8, 10] as conditions. Furthermore, conditional DMs have already been introduced in LLIE tasks and thus several successful attempts have emerged [14, 37, 48, 49, 57]. It is worth noting that sampling efficiency is a common difficulty for the diffusion model, where limited sampling steps result in subpar generation fidelity. Therefore, Jiang *et al.* [14] adopt 2D discrete wavelet transformations and utilize the low-resolution coefficients as conditions for faster inference speed. However, without the explicit modeling of color information, the results are unpleasing as shown in Fig. 1(a). To better adapt to LLIE task, the color map [34, 49, 57] and Retinex model [48] are introduced into the diffusion process. [34] and [49] try to maintain color

consistency, while they only apply an invariant color map and gain limited ability of enhancement. Zhou *et al.* [57] propose a pyramid diffusion model (PyDiff) to perform the reverse process by progressively increasing resolution and adjusting the color after denoising through a global corrector, which improves the visual quality to a certain extent as shown in Fig. 1(b). However, the visual results show limitations in preserving color and details, which may be solved by the solid Retinex theory. Thus, to facilitate the physical interpretability, Diff-Retinex [48] explores the possibility of establishing the Retinex-based diffusion model. The denoising network inputs reflectance and illumination maps as conditional images, and a consistent network is proposed to preserve the content, similar to PyDiff [57]. However, directly applying the decomposed maps as conditions is expected to be imperfect since Retinex theory is essentially an ideal model and the corruptions in reflectance and illumination need to be considered [1]. Although numerous studies have recognized the significance of auxiliary guidance in the diffusion process, they fail to explore a suitable strategy and still produce unfavorable visual results. Thus, the condition strategy has the potential for further improvement in establishing an LLIE-specific diffusion model with significant capability of enhancement.

To address the aforementioned issues, we propose a novel Retinex-conditioned diffusion model, ReCo-Diff, specially designed for the LLIE task. From a new perspective, we combine physical models and the conditioning technique to produce better results. Specifically, our ReCo-Diff learns the Retinex-based prior as extra pre-processing conditions in the diffusion model and refines the enhanced output by integrating the Retinex-based conditions as guidance, instead of processing the reflectance and illumination maps directly [48]. In each step, our ReCo-Diff conducts Retinex-based condition learning and conditional image refinement successively. In the stage of condition learning, we first utilize a pre-trained network (DNet) to produce initial decomposed maps. The adjustment network (ANet) improves the initial maps by suppressing noise in reflectance and adjusting exposure in illumination, and the outputs serve as reliable Retinex-based conditions for better refinement. Then, different from simply using color maps as conditional inputs [34, 49, 57], our ReCo-Diff incorporates the Retinex-based conditions into the denoising U-Net (UNet) for better conditional guidance. Furthermore, unlike [48, 57] directly using stacked convolutional layers to improve the enhanced image, we propose a refinement network (RNet) to better preserve color and contents based on the Retinex theory, which separates the illumination while maintaining the color and details in the reflectance. We reformulate the Retinex model into a residual manner to alleviate the corruptions and thus design the feature- and image-level Retinex-conditioned modules (F/IRCM) in the

RNet. The physically inspired conditions and the modified Retinex model for refinement endow our ReCo-Diff with the superior capability of enhancement. Finally, as shown in Fig. 1(c), our ReCo-Diff provides the most pleasing result by using the novel task-specific condition strategy.

The main contributions of our work are as follows:

- We propose a novel diffusion-based method for LLIE with a Retinex-based condition strategy, exploring the role of physical models in controlling the generation capabilities of diffusion models.
- We formulate our ReCo-Diff from two aspects: the condition learning stage that improves initial decomposed maps and produces reliable Retinex-based conditions; and the conditional refinement stage that exploits the Retinex-based conditions to guide the diffusion process for better preserving the color and contents.
- Extensive experiments on representative benchmarks demonstrate that the Retinex-based condition strategy and the well-designed learning and refinement process lead to the superior performance of our ReCo-Diff.

2. Related Work

Low-light Image Enhancement. Numerous works introduce the Retinex theory into deep neural networks [1, 5, 7, 21, 22, 39, 40, 48, 52, 53]. The Retinex-Net [39] is the most inspiring method combining physical model and DNNs. Then, Zhang *et al.* proposes KinD [52] and KinD++ [53] to provide more effective solutions. Rather than complex multi-stage training pipeline, Fu *et al.* [5] and Cai *et al.* [1] explore the possibility of end-to-end frameworks and achieve significant performance improvement.

Without Retinex theory, recent works concentrate on directly end-to-end manners [16, 26, 29, 36, 42–44, 50, 55]. LLNet [27] inspires the emergence of end-to-end methods. Primarily, supervised methods show promising capability of enhancement. For reducing color deviation, [20, 41, 45, 54] adopt 3DLUT and histogram to preserve color consistency. In [43, 44], the SNR-aware prior and the structure-aware features are taken as guidance to produce realistic results. Recently, the Ultra-High-Definition (UHD) images become popular. LLformer [35] and UHD-Four [24] are proposed to enhance UHD images and release UHD datasets to promote the following research. Furthermore, semi-supervised [29, 46], unsupervised [7, 15] and zero-shot learning [9, 23, 56] are valuable when training images are limited.

Diffusion-Based Image Restoration and Low-Light Image Enhancement. Diffusion models [13, 33] show promising capability in image generation tasks [2, 32]. For solving image processing tasks, diffusion-based methods employ conditional mechanism to incorporate the distorted images as guidance [25], such as colorization [31], super-resolution [32], restoration [4, 18, 28], and LLIE [14, 34,

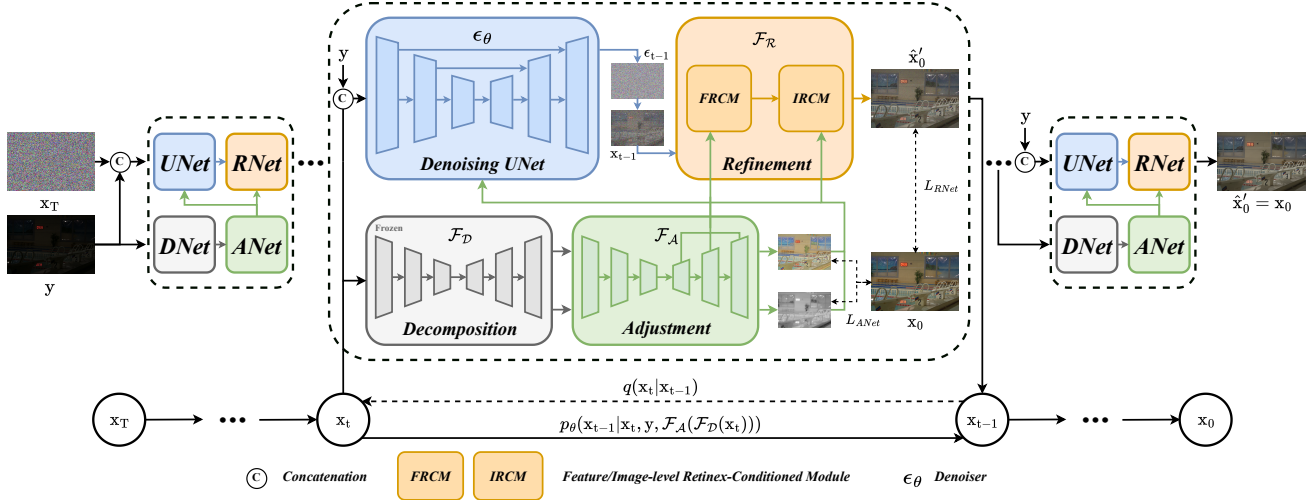


Figure 2. Overview of our Retinex-based conditional diffusion model (ReCo-Diff). Each step contains two stages: (a) In the learning stage, the pre-trained DNet provides the initial decomposed maps and the ANet adjusts and outputs reliable Retinex-based conditions. (b) In the refinement stage, the learned conditions are incorporated into UNet as extra inputs and are incorporated into RNet through F/IRCMs to preserve the color and content. FRCM and IRCM respectively receive the features and adjusted maps from ANet, detailed in Fig. 3.

37, 48, 49, 57]. To realize efficient diffusion-based LLIE, DiffLL [14] uses wavelet transformation to decrease the input size and a high-frequency restoration module to maintain the details. PyDiff [57] directly down-samples the image in early steps to speed up the sampling process. Considering the characteristics of LLIE task, LLDiffusion [34] and CLE-Diffusion [49] use the color map as extra conditional input to preserve the color information. Furthermore, PyDiff [57] proposes a global corrector to alleviate color degradation. By introducing Retinex theory, Diff-Retinex [48] decomposes the image and utilizes the reflectance and illumination maps as conditional images to form the guidance.

Although existing diffusion-based LLIE methods obtain good performance, they are limited by insufficient conditional guidance and produce unsatisfactory color and details. In this paper, we investigate a new condition strategy and propose ReCo-Diff to control the generative diffusion model by forming a Retinex-based conditional process, exploring a novel perspective for diffusion-based LLIE and achieving promising performance.

3. Method

The overview is shown in Fig. 2. We present the Retinex-based condition strategy to explore an effective diffusion-based method for LLIE. We introduce the conditional DDPM in Sec. 3.1 and present our ReCo-Diff in Sec. 3.2.

3.1. Conditional Denoising Diffusion Model

To deal with image restoration tasks, condition strategies are proposed to develop the conditional DDPM [25]. The conditional DDPM also generates a target image x_0 from a pure noise image x_T and refines the image through successive iterations. Unlike DDPM, the low-quality images are utilized as conditional inputs in conditional DDPM [32].

Thus, the conditional inference is defined as a reverse Markovian process:

$$p_\theta(\mathbf{x}_{0:T}|\mathbf{y}) = p(\mathbf{x}_T) \prod_{t=1}^T p_\theta(\mathbf{x}_{t-1}|\mathbf{x}_t, \mathbf{y}), \quad (1)$$

$$p_\theta(\mathbf{x}_{t-1}|\mathbf{x}_t, \mathbf{y}) = \mathcal{N}(\mathbf{x}_{t-1} | \mu_\theta(\mathbf{x}_t, \mathbf{y}, \gamma_t), \sigma_t^2 \mathbf{I}),$$

where $\gamma_t = \prod_{i=1}^t \alpha_i$ and $\alpha_{1:T}$ are scale parameters. Due to the absence of high-quality image x_0 in inference, ϵ_θ estimates noise and approximates x_0 as:

$$\hat{x}_0 = \frac{1}{\sqrt{\gamma_t}} \left(\mathbf{x}_t - \sqrt{1 - \gamma_t} \epsilon_\theta(\mathbf{x}_t, \mathbf{y}, \gamma_t) \right). \quad (2)$$

Therefore, the mean of $p_\theta(\mathbf{x}_{t-1}|\mathbf{x}_t, \mathbf{y})$ can be parameterized by applying the \hat{x}_0 into the posterior distribution [13]:

$$\mu_\theta(\mathbf{y}, \mathbf{x}_t, \gamma_t) = \frac{1}{\sqrt{\alpha_t}} \left(\mathbf{x}_t - \frac{1 - \alpha_t}{\sqrt{1 - \gamma_t}} \epsilon_\theta(\mathbf{x}_t, \mathbf{y}, \gamma_t) \right). \quad (3)$$

The training objective is to approximate the precise mean $\hat{\mu}_\theta$, which only optimizes the denoising network $\epsilon_\theta(\cdot)$. The overall optimization objective can be formulated as:

$$\mathbb{E}_{\mathbf{x}_0, \mathbf{y}, t, \epsilon \sim \mathcal{N}(0, \mathbf{I})} [\|\epsilon_t - \epsilon_\theta(\mathbf{x}_t, \mathbf{y}, \gamma_t)\|_2^2]. \quad (4)$$

3.2. Retinex-Based Conditional Diffusion Model

Retinex theory illustrates the assumption that the reflectance and illumination components can describe the original image, and the reflectance map is consistent under various lighting conditions. Low-/normal-light images $I, \hat{I} \in \mathbb{R}^{W \times H \times 3}$ share the constant $\hat{R} \in \mathbb{R}^{W \times H \times 3}$ and consist of diverse $L, \hat{L} \in \mathbb{R}^{W \times H \times 1}$ as:

$$I = \hat{R} \odot L, \quad \hat{I} = \hat{R} \odot \hat{L}, \quad (5)$$

where \odot denotes the element-wise multiplication. According to multi-scale Retinex [17], \hat{R} is the Retinex output by removing the lighting effects in I as follows:

$$\begin{aligned}\hat{R} &= \log(I) - \log(L) = \log(I) - \log(\mathcal{G}(I)), \\ \hat{I} &= \mathcal{T}(\exp(\hat{R})), \quad \hat{I} \in (0, 1),\end{aligned}\quad (6)$$

where $\mathcal{G}(\cdot)$ and $\mathcal{T}(\cdot)$ denote the convolution with the Gaussian surround function and the linear transformation function. However, although the ideal model maintains color constancy by estimating the reflectance map \hat{R} , details are easily broken through the removal of illumination. Thus, \hat{R} is more suitable to guide the color recovery. We introduce the low-light input to preserve the original information and reformulate Eq. (6) to model the process as:

$$\hat{I} = \mathcal{F}(I, \hat{R}), \quad (7)$$

where $\mathcal{F}(\cdot)$ denotes the deep network and \hat{R} acts as an auxiliary guidance. Inspired by the improved Retinex model, we consider the enhancement process from two stages: Retinex-based guidance adjustment and conditional image enhancement. Recalling the conditional DDPM model discussed in Sec. 3.1, the enhancement task can be performed due to the superiority of the generative model conditioned by low-light images [14, 34]. However, the noise and artifacts in low-light images inevitably mislead the diffusion model and cause detail loss and unsatisfactory color.

To mitigate this issue, we utilize the guided enhancement manner in Eq. (7) and integrate the Retinex-based priors into the diffusion process. Notably, color constancy can actually be affected by lighting variations and the corrupted R may lead to degradation of the enhanced image. Thus, we introduce the adjusted term $\hat{c} = \mathcal{F}_A(R, L)$, including more sufficient Retinex-based guidance and acting as priors in the conditional generation process. Subsequently, we formulate the enhancement model as:

$$\hat{I} = \mathcal{F}_R(\epsilon_\theta(I, \mathcal{F}_A(R, L)), \mathcal{F}_A(R, L)), \quad (8)$$

where $\epsilon_\theta(\cdot)$, $\mathcal{F}_R(\cdot)$, and $\mathcal{F}_A(\cdot)$ denote UNet, RNet, and ANet in Fig. 2, respectively. Combining the promising texture generation capability of the diffusion model and the conscious representation with vivid color and detail of Retinex theory, we develop a Retinex-based condition strategy for the conditional DDPM and formulate our ReCo-Diff. Eq. (8) represents the denoising and refinement process in one iteration, which can be described as two stages, Retinex-based condition learning and Retinex-conditioned refinement. In the first stage, we obtain the decomposition results from a pre-trained DNet and input them into the following ANet to produce Retinex-based conditions, which will be described in Sec. 3.2.1. Then, the conditions will be introduced into the UNet and RNet to achieve conditional image denoising and refinement as elaborated in Sec. 3.2.2.

3.2.1 Retinex-based Condition Learning

As described in Sec. 3.2, the basis of conditional image refinement is to learn high-quality conditions. Inspired by Retinex-based methods [39, 52], we propose the DNet to serve as a pre-processing module and produce initial

Retinex-based conditions. Compared to calculating an invariant color map as conditional input [34, 49], the decomposed maps contain not only color information but also details and illumination, achieving a more sufficient form of conditional inputs. To further exploit the progressively refined images in the diffusion process, DNet inputs \mathbf{x}_t as well and provides competent updated predictions R_{t-1} and L_{t-1} for better generation. However, the images in the early steps contain incorrect contents and mislead the decomposition. Therefore, an adjustment network (ANet) is introduced to deal with corruption and ameliorate the low-quality conditions in the early steps, achieving approving conditional enhancement during the whole generative process. Thus, we realize the Retinex-based condition learning as:

$$\hat{c}_{t-1} = \mathcal{F}_A(\mathbf{c}_{t-1}) = \mathcal{F}_A(\mathcal{F}_D(\mathbf{y}, \mathbf{x}_t)). \quad (9)$$

Pre-trained DNet. DNet adopts a lightweight UNet-like network to learn the decomposition mapping. It inputs the images I and outputs the reflectance R and illumination L . Inspired by the training strategy in [39], we utilize the constant reflectance loss, smooth illumination loss, and reconstruction loss to pre-train DNet. More details can be seen in the [supplementary materials](#).

Condition Adjustment. Directly using the initial decomposed maps with noise and inaccurate brightness may affect the diffusion process. Thus, we utilize the ANet to adjust the decomposition priors. The ANet employs a similar architecture to the DNet with tiny modifications on input and output layers. It inputs the initial maps $\mathbf{c}_t = [R_t, L_t]$ and learns to produce the adjusted $\hat{\mathbf{c}}_t = [R'_t, L'_t]$ from two aspects. We first aim to suppress the noise and calibrate the color in R_t by the joint adjustment loss:

$$\mathcal{L}_{ja} = \|R'_t - \hat{R}\|_1 + SSIM(R'_t, \hat{R}). \quad (10)$$

Then, we propose the joint exposure loss to adjust the sub-optimal illumination as follows:

$$\mathcal{L}_{je} = \|L'_t - \hat{L}\|_1 + Hist(L'_t, \hat{L}), \quad (11)$$

where $Hist(\cdot)$ denotes the L1 loss between the histogram of L'_t and ground-truth \hat{L} . Thus, the ANet is trained as:

$$\mathcal{L}_{ANet} = \lambda_{ja}\mathcal{L}_{ja} + \lambda_{je}\mathcal{L}_{je}, \quad (12)$$

where \mathcal{L}_{ANet} is the only loss to propagate gradient for smooth optimization by detaching R'_t and L'_t . Subsequently, ANet learns the progressive adjustment mapping of reflectance and illumination by incorporating time embedding and provides $\hat{\mathbf{c}}_t$. Furthermore, the multi-scale features F_t are crucial to fully exploit the learned mapping. Thus, the features are included in conditions as $\hat{\mathbf{c}}_t = [R'_t, L'_t, F_t]$, providing better lightness and color guidance.

3.2.2 Retinex-conditioned Refinement

After obtaining the Retinex-based conditions $\hat{\mathbf{c}}_t$, the next stage is to incorporate the conditions into the iterative diffusion process. Previous methods propose to introduce the invariant color maps [34, 49, 57] and Retinex decomposi-

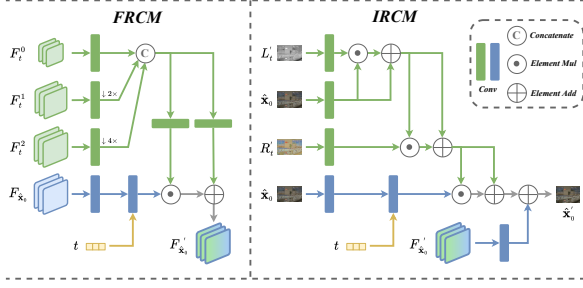


Figure 3. The architecture of the feature/image-level Retinex-conditioned modules (F/IRCM). FRCM inputs multi-scale features F_t from ANet and obtains the optimized image feature $F_{\hat{x}_0}'$. Then, IRCM inputs the R_t' , L_t' and the $F_{\hat{x}_0}'$ to refine the approximated \hat{x}_0 to produce the final output \hat{x}_0' .

tion [48]. However, existing condition strategies are insufficient to conduct the favorable iterative enhancement. In our ReCo-Diff, we already learn the Retinex-based conditions as described in Sec. 3.2.1. Then, following the usage of color map [34, 49], we first control the generation capability of UNet by leveraging \hat{c}_t as extra inputs, while the carefully prepared conditions are being underutilized just for denoising. Thus, as illustrated in Eq. (8), we apply a post-processing refinement network (RNet) to fully exploit the conditions and guarantee the consistent color and contents of \hat{x}_0' . Different from [48], RNet adopts a lightweight architecture and implements Retinex-conditioned refinement at both feature- and image-levels by FRCM and IRCM. Overall, the refinement stage can be elaborated as:

$$\hat{x}_0' = \mathcal{F}_R(\epsilon_\theta(\mathbf{x}_{t-1}, \hat{c}_t), \hat{c}_t), \quad (13)$$

where \hat{x}_0' denotes the output refined by RNet at time step t .

Conditional Denoising. UNet introduces reflectance and illumination maps through embedding layers and integrates them in feature space instead of concatenation for effective information interaction. Specifically, we first transform the original $R_t' \in \mathbb{R}^{W \times H \times 3}$ and $L_t' \in \mathbb{R}^{W \times H \times 1}$ into embedding features R_{em} and L_{em} . To maintain the content and color information, the reflectance embedding $R_{em} \in \mathbb{R}^{W \times H \times C}$ keeps the original resolution. Moreover, the illumination embedding is downsampled as $L_{em} \in \mathbb{R}^{W/2 \times H/2 \times C}$ for computational efficiency thanks to the smooth distribution of lightness. Then, the R_{em} and L_{em} are input to the conditional layers with original and half sizes respectively, guiding the denoising process. Thus, we can approximate \hat{x}_0 by updating Eq. (2) as:

$$\hat{x}_0 = \frac{1}{\sqrt{\gamma_t}} \left(\mathbf{x}_t - \sqrt{1 - \gamma_t} \epsilon_\theta(\mathbf{x}_t, \mathbf{y}, \hat{c}_t, \gamma_t) \right). \quad (14)$$

Conditional Refinement. As shown in Fig. 2, RNet consists of two Retinex-conditioned modules to realize the color recovery and detail enhancement of the approximated \hat{x}_0 . Specifically, we first implement the Retinex-conditioned refinement in feature space, since F_t incorporates rich information of adjustment mapping as illustrated

in Sec. 3.2.1. Thus, as depicted in Fig. 3, we unify the sizes of multi-scale features in F_t and model them as affine transformation parameters F_γ and F_β . Then, the feature fusion is carried out by scaling and shifting operations $\mathcal{F}_T(\cdot|\cdot)$ as:

$$F_{\hat{x}_0}' = \mathcal{F}_T(F_{\hat{x}_0}|F_t) = F_\gamma \odot W(F_{\hat{x}_0}) + F_\beta, \quad (15)$$

where W denotes the convolution layer and \odot is the dot product. However, although the FRCM and conditional layers in UNet integrate the Retinex-based priors into the diffusion process, applying the calculation of the superior Retinex model can further refine the enhanced result. Therefore, as shown in Fig. 3, we conduct refinement at image-level by introducing R_t' and L_t' into IRCM. To simultaneously alleviate the errors resulting from the ideal model and establish a stable training process, we reformulate Eq. (6) into a residual refinement manner as:

$$\begin{aligned} \Delta \hat{x}_0 &= \mathcal{F}_T(R_t' | \mathcal{F}_T(L_t' | \hat{x}_0)), \\ \hat{x}_0' &= \mathcal{F}_T(\hat{x}_0 | \Delta \hat{x}_0) + W(F_{\hat{x}_0}'), \end{aligned} \quad (16)$$

where \hat{x}_0' is the final refined output of RNet. In RNet, FRCM and IRCM fully exploit the Retinex-based conditions and produce results with consistent color and details. Accordingly, in addition to Eq. (4), we also utilize the constraint of \hat{x}_0' to optimize the ReCo-Diff as follows:

$$\mathcal{L}_{RNet} = \mathbb{E}_{\mathbf{x}_0, \mathbf{y}, t, \epsilon \sim \mathcal{N}(0, \mathbf{I})} [\|\mathbf{x}_0 - \mathcal{F}_R(\hat{x}_0, \hat{c}_t, \gamma_t)\|_2^2]. \quad (17)$$

4. Experiments

4.1. Experimental Settings

Implementation Details. Our method is trained using an NVIDIA RTX A100 GPU and the training iteration is set to 600k. We use the Adam optimizer with the momentum as (0.9, 0.999). The initial learning rate is set to 1×10^{-4} and decays by a factor of 0.5 after every 1×10^5 iterations. The batch size and patch size are set to 8 and 256×256 , respectively. We followed the similar architecture of [32] as our denoising U-Net ϵ_θ . We used 2000 diffusion steps T for training. In the inference stage, we follow the DDIM [33] and set 8 steps for enhancement.

Datasets. We evaluate the proposed method on several datasets from various scenes, including LOL [39], LOL-v2 [47], and UHD-LL [24]. The LOL dataset [39] includes 485 low/normal-light image pairs for training and 15 pairs for testing. The LOL-v2 dataset [47] can be divided into two parts, the real part is an extension of LOL with 689/100 pairs and the synthetic part includes 900/100 pairs for training and testing. The UHD-LL dataset [24] includes 2000 pairs for training and 150 pairs for testing.

Metrics. To conduct comparison, we employ two full-reference metrics peak signal-to-noise ratio (PSNR) and structural similarity (SSIM) [38], and two perceptual metrics learned perceptual image patch similarity (LPIPS) [51], Fréchet Inception Distance (FID) [12] for evaluation.

Table 1. Quantitative comparison on the LOL [39] and LOL-v2-real [47] datasets. \uparrow (\downarrow) denotes that, larger (smaller) values suggest better quality. The best results are highlighted in **bold** and the second best results are in underline (Special fonts are also used in Tabs. 2 and 3).

Methods	LOL				LOL-v2-real			
	PSNR \uparrow	SSIM \uparrow	LPIPS \downarrow	FID \downarrow	PSNR \uparrow	SSIM \uparrow	LPIPS \downarrow	FID \downarrow
LIME [11] TIP'16	16.760	0.560	0.350	117.892	15.240	0.470	0.428	118.171
RetinexNet [39] BMVC'18	16.770	0.462	0.474	113.699	18.371	0.723	0.365	133.905
KinD [52] MM'19	20.870	0.799	0.207	104.632	17.544	0.669	0.375	137.346
DRBN [46] CVPR'20	19.860	0.834	0.155	75.359	20.130	0.830	0.147	60.631
Zero-DCE [9] CVPR'20	14.861	0.562	0.335	101.237	18.059	0.580	0.313	91.939
MIRNet [50] PAMI'22	24.140	0.842	0.131	69.179	20.357	0.782	0.317	49.108
SNR [43] CVPR'22	24.608	0.840	0.151	55.121	21.479	0.848	0.157	54.532
LLFlow [36] AAAI'22	24.999	0.870	0.117	65.143	26.200	<u>0.888</u>	0.137	69.793
PairLIE [7] CVPR'23	19.510	0.736	0.248	100.715	20.357	0.782	0.317	96.911
SMG [44] CVPR'23	23.684	0.826	0.118	58.846	24.620	0.867	0.148	78.582
FourLLIE [24] MM'23	20.222	0.766	0.250	91.793	22.340	0.847	0.051	89.334
Retinexformer [1] ICCV'23	25.153	0.843	0.131	71.148	22.794	0.839	0.171	62.439
Diff-Retinex [48] ICCV'23	21.981	0.863	0.048	<u>47.851</u>	-	-	-	-
DiffLL [14] SIGGRAPH Asia'23	26.336	0.845	0.217	48.114	<u>28.857</u>	0.876	0.207	45.359
PyDiff [57] IJCAI'23	27.088	0.875	0.111	56.215	27.236	0.869	0.211	57.832
ReCo-Diff (Ours)	27.626	0.884	<u>0.090</u>	42.990	29.306	0.906	<u>0.105</u>	<u>46.677</u>

Table 2. Quantitative comparison on the LOL-v2-synthetic [47].

Methods	LOL-v2-synthetic			
	PSNR \uparrow	SSIM \uparrow	LPIPS \downarrow	FID \downarrow
LIME [11] TIP'16	16.880	0.758	0.104	-
RetinexNet [39] BMVC'18	16.551	0.652	0.379	98.843
KinD [52] MM'19	18.956	0.801	0.262	89.156
DRBN [46] CVPR'20	21.687	0.825	0.174	52.972
Zero-DCE [9] CVPR'20	17.756	0.814	0.168	49.239
MIRNet [50] PAMI'22	21.941	0.876	0.112	38.775
SNR [43] CVPR'22	24.130	0.927	0.032	23.971
LLFlow [36] AAAI'22	23.692	0.911	0.103	32.576
PairLIE [7] CVPR'23	19.074	0.794	0.230	85.209
SMG [44] CVPR'23	25.618	0.905	0.053	23.210
FourLLIE [24] MM'23	24.649	0.919	<u>0.039</u>	26.351
RetinexFormer [1] ICCV'23	25.670	<u>0.928</u>	0.059	<u>22.781</u>
DiffLL [14] SIGGRAPH Asia'23	25.456	0.896	0.102	43.670
PyDiff [57] IJCAI'23	<u>26.038</u>	0.922	0.072	26.854
ReCo-Diff (Ours)	26.701	0.935	0.057	22.755

Compared Methods. We compare with a rich collection of state-of-the-art methods, including LIME [11], RetinexNet [39], KinD [52], DRBN [46], Zero-DCE [9], EnlightGAN [15], MIRNet [50], SNR [43], LLFlow [36], PairLIE [7], SMG [44], FourLLIE [24], Retinexformer [1], UHDFour [24] and diffusion-based methods including Diff-Retinex [48], DiffLL [14], and PyDiff [57].

4.2. Quantitative Evaluation

Tabs. 1 to 3 show the comparisons on LOL, LOL-v2, and UHD-LL. It is clear that our ReCo-Diff achieves consistent and significant performance gain over all competing methods. Specifically, our method provides significant improvement of 0.638dB/0.449dB on LOL/LOL-v2 datasets respectively, establishing the new state-of-the-art with PSNR values of 27.626dB/29.306dB. Furthermore, our method achieves similar performance in terms of SSIM, yielding the best values of 0.884/0.906. On the LOL-v2-synthetic test set, our ReCo-Diff improves the PSNR and SSIM by 0.663 and 0.013 than the second-best method. On UHD-LL, we also achieve considerable performance on PSNR and SSIM

Table 3. Quantitative comparison on the UHD-LL [24]. To conserve space, we select recent methods in 2023 while ensuring that the results are sufficient to demonstrate our superiority.

Methods	UHD-LL			
	PSNR \uparrow	SSIM \uparrow	LPIPS \downarrow	FID \downarrow
SMG [44] CVPR'23	25.852	0.869	0.248	41.647
FourLLIE [24] MM'23	22.462	0.814	0.296	61.380
UHDFour [24] ICLR'23	<u>26.226</u>	<u>0.900</u>	0.239	39.956
DiffLL [14] SIGGRAPH Asia'23	24.330	0.843	0.245	49.098
PyDiff [57] IJCAI'23	25.753	0.897	<u>0.159</u>	<u>36.263</u>
ReCo-Diff (Ours)	27.347	0.912	0.121	27.233

of 1.121dB and 0.012, proving our capability of generalization. Although our ReCo-Diff obtains several second-best LPIPS and FID values, it outperforms other diffusion-based LLIE methods in most cases and achieves the best FID on LOL, which indicates the overall performance on perceptual metrics is still competitive. Consequently, the considerable performance shows the capability of suppressing noise and preserving color and details by Retinex-based priors, which demonstrates the effectiveness of our proposed Retinex-based condition strategy in resolving LLIE task.

4.3. Qualitative Evaluation

The qualitative evaluations on LOL and LOL-v2 are shown in Figs. 1, 4 and 5. As indicated by the visual comparisons, our ReCo-Diff shows superior enhancement capability and generates images with more pleasing perceptual quality. Specifically, in the first row of Fig. 4, previous methods fail to reconstruct the detailed textures of the blanket, while our ReCo-Diff provides rich details and mitigates the color gap. As for images of the middle row, although most methods enhance the white regions well, they produce incorrect color and artifacts in the regions with complex scenes. Notably, our method not only restores the print on the carton but preserves the color consistency. Furthermore, the bottom row exhibits that our ReCo-Diff is capable of recovering the vulnerable content vanishing in the results of other methods, which reasonably indicates the superior capacity

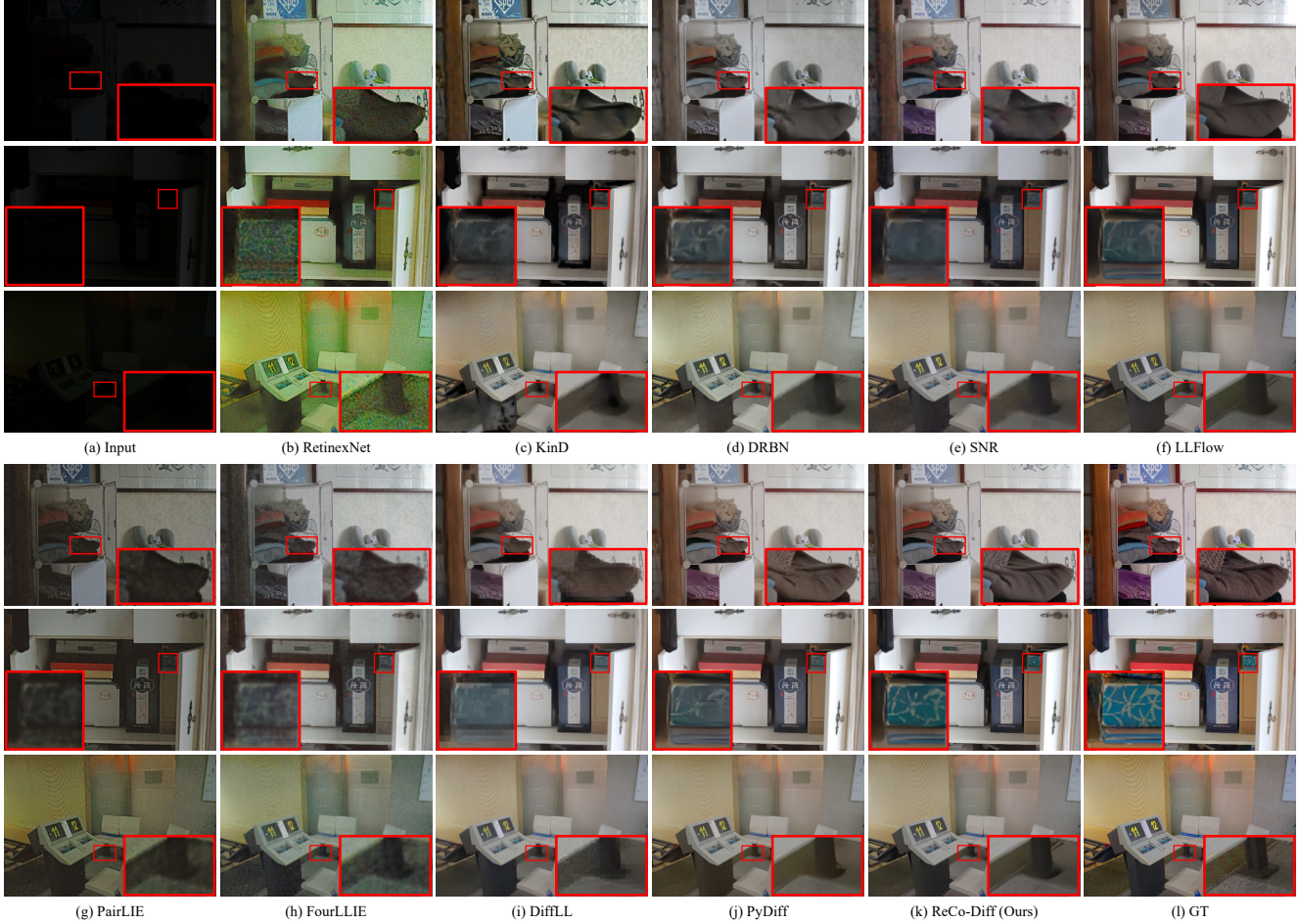


Figure 4. Visual comparison of our ReCo-Diff and the compared LLIE methods on the LOL dataset.



Figure 5. Visual comparison of our ReCo-Diff and the compared LLIE methods on the UHD-LL dataset.

of restoring naturalistic details. In Fig. 5, although PyDiff [57] shows a similar overall look to ours, the ReCo-Diff enhances the green cup and the red text with correct color and better saturation. Hence, our ReCo-Diff yields more visually pleasing results as compared to baselines, supporting our method’s excellent performance in quantitative evaluation. More results are provided in [supplementary material](#).

4.4. Ablation Study

Contribution of ANet, RNet, and Conditional UNet. As shown in Tab. 4, we conduct experiments of several ablation settings by removing different components from the framework individually. The “w/o UNet-Cond” denotes the removal of conditional layers in the UNet. Compared with all ablation settings, our full setting yields the best performance. In the case of the removal of FRCM leads to the decrease of PSNR value by an average of 0.364dB below the

baseline, which demonstrates the effectiveness of introducing the multi-scale features from ANet into the refinement process. The comparison between “w/o UNet-Cond” and the baseline shows a similar degradation level, resulting in an average reduction of 0.349dB, which proves the necessity of integrating Retinex features into the denoising network. Notably, by comparing “w/o IRCM” and “w/ ALL”, we observe a significant decline that surpasses the aforementioned two cases, which serves to highlight the crucial role of our IRCM owing to its well-designed residual refinement manner. Furthermore, the comparison between all cases under “w/ ANet” and “w/o ANet” exhibits an average drop of 0.272dB on PSNR, illustrating that the better Retinex-based condition provided by ANet eventually improves the visual quality of generated images.

Additionally, results in Fig. 6 depict that “w/o FRCM”

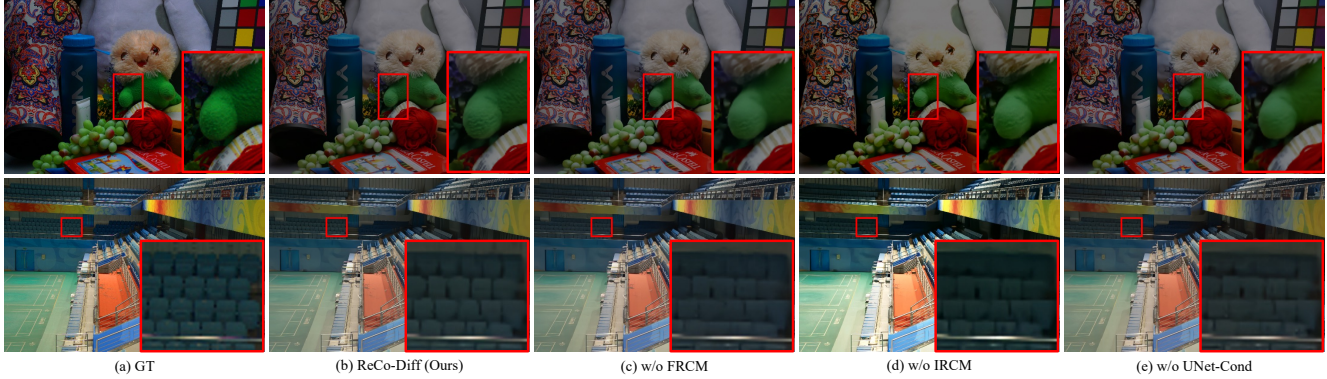


Figure 6. Visual comparison on the LOL/LOL-v2 datasets for investigating the contribution of key techniques of our ReCo-Diff.

Table 4. Ablation studies on LOL for investigating the contribution of key techniques both in the learning and refinement stages.

Learning	Refinement	PSNR \uparrow	SSIM \uparrow	LPIPS \downarrow
w/ ANet	w/ ALL	27.626	0.884	0.090
	w/o FRCM	27.344	0.875	0.112
	w/o IRCM	27.262	0.872	0.119
	w/o UNet-Cond	27.278	0.875	0.113
w/o ANet	w/ ALL	27.301	0.877	0.103
	w/o FRCM	26.956	0.869	0.131
	w/o IRCM	26.783	0.864	0.140
	w/o UNet-Cond	26.967	0.868	0.134

Table 5. Ablation studies of training settings of ANet for investigating the effects of the joint loss function.

Settings	LOL			LOL-v2-real		
	PSNR \uparrow	SSIM \uparrow	LPIPS \downarrow	PSNR \uparrow	SSIM \uparrow	LPIPS \downarrow
w/ Both	27.626	0.884	0.090	29.306	0.906	0.105
w/o SSIM	27.502	0.875	0.101	29.163	0.891	0.118
w/o Hist	27.508	0.875	0.102	29.156	0.892	0.119
w/o Both	27.446	0.872	0.106	29.061	0.885	0.124

and “UNet-Cond” lead to the reduction of regions with detailed textures, such as uneven surfaces and closely arranged chairs. Although “w/o IRCM” preserves details better, the lack of direct guidance of Retinex components induces the color shift and unnatural illumination. Fig. 7 shows that ANet reduces the noise (top rows) and enhances the illumination (bottom rows) in early steps, and improves the quality of Retinex-based conditions in the whole process.

Joint Losses of ANet. Tab. 5 lists the results of different settings for training ANet. The “w/ Both” and “w/o Both” denote that using the original \mathcal{L}_{ja} and \mathcal{L}_{je} and removing both SSIM loss and Hist loss, respectively. First, “w/ Both” reasonably achieves the best performance compared with all ablation settings. The settings of “w/o SSIM” and “w/o Hist” show degradation on all metrics, demonstrating the effects of SSIM loss and Hist loss respectively. Comparing “w/ Both” and “w/o Both” shows a favorable gain of 0.210dB and illustrates the necessity of using the constraint of both the structure and histogram. Furthermore, we can see the effects of SSIM loss and Hist loss by comparing Retinex output at step 8 in Fig. 7. The reflectance and illu-

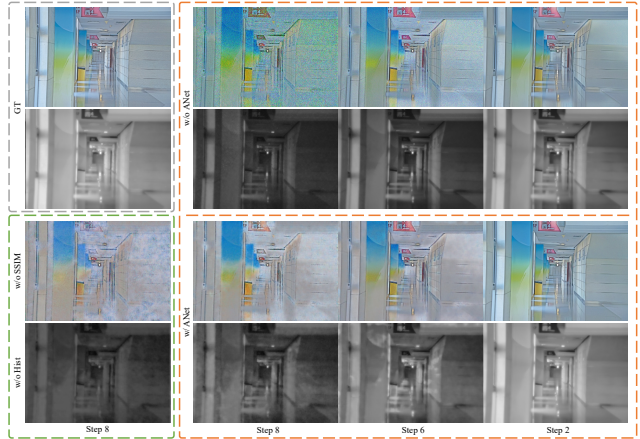


Figure 7. Ablation study of ANet in terms of reflectance (row 1,3) and illumination (row 2,4) maps. Images in orange box shows the effects of ANet corresponding to Tab. 4, and green box shows the effects of SSIM and Hist loss corresponding to Tab. 5.

mination maps in the green box contain more artifacts and unsatisfactory brightness distribution. More ablation studies and analysis are provided in [supplementary material](#).

5. Conclusion

In this paper, we propose an LLIE-specific diffusion model with a Retinex-based condition strategy, ReCo-Diff, for low-light image enhancement. Our ReCo-Diff combines Retinex theory and diffusion model in two stages: Retinex-based condition learning and conditional refinement. In the learning stage, we utilize DNet to obtain the initial priors and then provide robust Retinex-based conditions by ANet. In the refinement stage, the prepared conditions are integrated into both UNet and RNet through conditional layers and RCMs to control the diffusion process and produce better color and details. Extensive experiments demonstrate that our ReCo-Diff outperforms state-of-the-art methods on representative benchmarks. We also hope to encourage more attention to develop DMs incorporating intrinsic characteristics of low-level vision.

References

- [1] Yuanhao Cai, Hao Bian, Jing Lin, Haoqian Wang, Radu Timofte, and Yulun Zhang. Retinexformer: One-stage Retinex-based transformer for low-light image enhancement. In *ICCV*, pages 12504–12513, 2023. 2, 6
- [2] Jooyoung Choi, Sungwon Kim, Yonghyun Jeong, Youngjune Gwon, and Sungroh Yoon. ILVR: Conditioning method for denoising diffusion probabilistic models. *arXiv preprint arXiv:2108.02938*, 2021. 2
- [3] Jiankang Deng, Jia Guo, Niannan Xue, and Stefanos Zafeiriou. ArcFace: Additive angular margin loss for deep face recognition. In *CVPR*, pages 4690–4699, 2019. 1
- [4] Ben Fei, Zhaoyang Lyu, Liang Pan, Junzhe Zhang, Weidong Yang, Tianyue Luo, Bo Zhang, and Bo Dai. Generative diffusion prior for unified image restoration and enhancement. In *CVPR*, pages 9935–9946, 2023. 2
- [5] Huiyuan Fu, Wenkai Zheng, Xiangyu Meng, Xin Wang, Chuanming Wang, and Huadong Ma. You do not need additional priors or regularizers in Retinex-based low-light image enhancement. In *CVPR*, pages 18125–18134, 2023. 2
- [6] Jun Fu, Jing Liu, Haijie Tian, Yong Li, Yongjun Bao, Zhiwei Fang, and Hanqing Lu. Dual attention network for scene segmentation. In *CVPR*, pages 3146–3154, 2019. 1
- [7] Zhenqi Fu, Yan Yang, Xiaotong Tu, Yue Huang, Xinghao Ding, and Kai-Kuang Ma. Learning a simple low-light image enhancer from paired low-light instances. In *CVPR*, pages 22252–22261, 2023. 2, 6
- [8] Sicheng Gao, Xuhui Liu, Bohan Zeng, Sheng Xu, Yanjing Li, Xiaoyan Luo, Jianzhuang Liu, Xiantong Zhen, and Baochang Zhang. Implicit diffusion models for continuous super-resolution. In *CVPR*, pages 10021–10030, 2023. 1
- [9] Chunle Guo, Chongyi Li, Jichang Guo, Chen Change Loy, Junhui Hou, Sam Kwong, and Runmin Cong. Zero-reference deep curve estimation for low-light image enhancement. In *CVPR*, pages 1780–1789, 2020. 2, 6
- [10] Lanqing Guo, Chong Wang, Wenhan Yang, Siyu Huang, Yufei Wang, Hanspeter Pfister, and Bihan Wen. Shadowdiffusion: When degradation prior meets diffusion model for shadow removal. In *CVPR*, pages 14049–14058, 2023. 1
- [11] Xiaojie Guo, Yu Li, and Haibin Ling. LIME: Low-light image enhancement via illumination map estimation. *TIP*, 26: 982–993, 2016. 6
- [12] Martin Heusel, Hubert Ramsauer, Thomas Unterthiner, Bernhard Nessler, and Sepp Hochreiter. Gans trained by a two time-scale update rule converge to a local nash equilibrium. *NIPS*, 30, 2017. 5
- [13] Jonathan Ho, Ajay Jain, and Pieter Abbeel. Denoising diffusion probabilistic models. *NIPS*, 33:6840–6851, 2020. 1, 2, 3
- [14] Hai Jiang, Ao Luo, Songchen Han, Haoqiang Fan, and Shuaicheng Liu. Low-light image enhancement with wavelet-based diffusion models. *arXiv preprint arXiv:2306.00306*, 2023. 1, 2, 3, 4, 6
- [15] Yifan Jiang, Xinyu Gong, Ding Liu, Yu Cheng, Chen Fang, Xiaohui Shen, Jianchao Yang, Pan Zhou, and Zhangyang Wang. EnlightenGAN: Deep light enhancement without paired supervision. *TIP*, 30:2340–2349, 2021. 2, 6
- [16] Xin Jin, Ling-Hao Han, Zhen Li, Chun-Le Guo, Zhi Chai, and Chongyi Li. DNF: Decouple and feedback network for seeing in the dark. In *CVPR*, pages 18135–18144, 2023. 2
- [17] Daniel J Jobson, Zia-ur Rahman, and Glenn A Woodell. A multiscale Retinex for bridging the gap between color images and the human observation of scenes. *TIP*, 6:965–976, 1997. 3
- [18] Bahjat Kawar, Michael Elad, Stefano Ermon, and Jiaming Song. Denoising diffusion restoration models. *NIPS*, 35: 23593–23606, 2022. 2
- [19] Mikhail Kennerley, Jian-Gang Wang, Bharadwaj Veeravalli, and Robby T Tan. 2PCNet: Two-phase consistency training for day-to-night unsupervised domain adaptive object detection. In *CVPR*, pages 11484–11493, 2023. 1
- [20] Bomi Kim, Sunhyeok Lee, Nahyun Kim, Donggon Jang, and Dae-Shik Kim. Learning color representations for low-light image enhancement. In *WACV*, pages 1455–1463, 2022. 2
- [21] Chongyi Li, Jichang Guo, Fatih Porikli, and Yanwei Pang. LightenNet: A convolutional neural network for weakly illuminated image enhancement. *RPL*, 2018. 2
- [22] Chongyi Li, Chunle Guo, Ling-Hao Han, Jun Jiang, Ming-Ming Cheng, Jinwei Gu, and Chen Change Loy. Low-light image and video enhancement using deep learning: A survey. *TPAMI*, 2021. 2
- [23] Chongyi Li, Chunle Guo, and Chen Change Loy. Learning to enhance low-light image via zero-reference deep curve estimation. *TPAMI*, 2021. 2
- [24] Chongyi Li, Chun-Le Guo, Man Zhou, Zhexin Liang, Shangchen Zhou, Ruicheng Feng, and Chen Change Loy. Embedding fourier for ultra-high-definition low-light image enhancement. In *ICLR*, 2023. 2, 5, 6
- [25] Xin Li, Yulin Ren, Xin Jin, Cuiling Lan, Xingrui Wang, Wenjun Zeng, Xinchao Wang, and Zhibo Chen. Diffusion models for image restoration and enhancement—A comprehensive survey. *arXiv preprint arXiv:2308.09388*, 2023. 2, 3
- [26] Seokjae Lim and Wonjun Kim. DSLR: Deep stacked Laplacian restorer for low-light image enhancement. *TMM*, 23: 4272–4284, 2020. 2
- [27] Kin Gwn Lore, Adedotun Akintayo, and Soumik Sarkar. LLNet: A deep autoencoder approach to natural low-light image enhancement. *PR*, 61:650–662, 2017. 2
- [28] Ziwei Luo, Fredrik K Gustafsson, Zheng Zhao, Jens Sjölund, and Thomas B Schön. Image restoration with mean-reverting stochastic differential equations. *arXiv preprint arXiv:2301.11699*, 2023. 1, 2
- [29] Sameer Malik and Rajiv Soundararajan. Semi-supervised learning for low-light image restoration through quality assisted pseudo-labeling. In *WACV*, pages 4105–4114, 2023. 2
- [30] Axi Niu, Kang Zhang, Trung X Pham, Jinqiu Sun, Yu Zhu, In So Kweon, and Yanning Zhang. CDPMSR: Conditional diffusion probabilistic models for single image super-resolution. *arXiv preprint arXiv:2302.12831*, 2023. 1
- [31] Chitwan Saharia, William Chan, Huiwen Chang, Chris Lee, Jonathan Ho, Tim Salimans, David Fleet, and Mohammad Norouzi. Palette: Image-to-image diffusion models. In

- ACM SIGGRAPH 2022 Conference Proceedings*, pages 1–10, 2022. 1, 2
- [32] Chitwan Saharia, Jonathan Ho, William Chan, Tim Salimans, David J Fleet, and Mohammad Norouzi. Image super-resolution via iterative refinement. *TPAMI*, 45(4):4713–4726, 2022. 2, 3, 5
- [33] Jiaming Song, Chenlin Meng, and Stefano Ermon. Denoising diffusion implicit models. *arXiv preprint arXiv:2010.02502*, 2020. 1, 2, 5
- [34] Tao Wang, Kaihao Zhang, Ziqian Shao, Wenhan Luo, Bjorn Stenger, Tae-Kyun Kim, Wei Liu, and Hongdong Li. LLD-diffusion: Learning degradation representations in diffusion models for low-light image enhancement. *arXiv preprint arXiv:2307.14659*, 2023. 1, 2, 3, 4, 5
- [35] Tao Wang, Kaihao Zhang, Tianrun Shen, Wenhan Luo, Bjorn Stenger, and Tong Lu. Ultra-high-definition low-light image enhancement: A benchmark and transformer-based method. In *AAAI*, pages 2654–2662, 2023. 2
- [36] Yufei Wang, Renjie Wan, Wenhan Yang, Haoliang Li, Lap-Pui Chau, and Alex Kot. Low-light image enhancement with normalizing flow. In *AAAI*, pages 2604–2612, 2022. 2, 6
- [37] Yufei Wang, Yi Yu, Wenhan Yang, Lanqing Guo, Lap-Pui Chau, Alex C Kot, and Bihan Wen. ExposureDiffusion: Learning to expose for low-light image enhancement. In *ICCV*, pages 12438–12448, 2023. 1, 3
- [38] Zhou Wang, Alan C Bovik, Hamid R Sheikh, and Eero P Simoncelli. Image quality assessment: From error visibility to structural similarity. *TIP*, 13:600–612, 2004. 5
- [39] Chen Wei, Wenjing Wang, Wenhan Yang, and Jiaying Liu. Deep retinex decomposition for low-light enhancement. In *BMVC*, 2018. 2, 4, 5, 6
- [40] Wenhui Wu, Jian Weng, Pingping Zhang, Xu Wang, Wenhan Yang, and Jianmin Jiang. URetinex-Net: Retinex-based deep unfolding network for low-light image enhancement. In *CVPR*, pages 5901–5910, 2022. 2
- [41] Yuhui Wu, Chen Pan, Guoqing Wang, Yang Yang, Jiwei Wei, Chongyi Li, and Heng Tao Shen. Learning semantic-aware knowledge guidance for low-light image enhancement. In *CVPR*, pages 1662–1671, 2023. 2
- [42] Ke Xu, Xin Yang, Baocai Yin, and Rynson WH Lau. Learning to restore low-light images via decomposition-and-enhancement. In *CVPR*, pages 2281–2290, 2020. 2
- [43] Xiaogang Xu, Ruixing Wang, Chi-Wing Fu, and Jiaya Jia. SNR-aware low-light image enhancement. In *CVPR*, pages 17714–17724, 2022. 2, 6
- [44] Xiaogang Xu, Ruixing Wang, and Jiangbo Lu. Low-light image enhancement via structure modeling and guidance. In *CVPR*, pages 9893–9903, 2023. 2, 6
- [45] Canqian Yang, Meiguang Jin, Xu Jia, Yi Xu, and Ying Chen. AdaInt: Learning Adaptive Intervals for 3D Lookup Tables on Real-time Image Enhancement. In *CVPR*, pages 17522–17531, 2022. 2
- [46] Wenhan Yang, Shiqi Wang, Yuming Fang, Yue Wang, and Jiaying Liu. From fidelity to perceptual quality: A semi-supervised approach for low-light image enhancement. In *CVPR*, pages 3063–3072, 2020. 2, 6
- [47] Wenhan Yang, Wenjing Wang, Haofeng Huang, Shiqi Wang, and Jiaying Liu. Sparse gradient regularized deep Retinex network for robust low-light image enhancement. *TIP*, 30:2072–2086, 2021. 5, 6
- [48] Xunpeng Yi, Han Xu, Hao Zhang, Linfeng Tang, and Jiayi Ma. Diff-Retinex: Rethinking low-light image enhancement with a generative diffusion model. In *ICCV*, pages 12302–12311, 2023. 1, 2, 3, 5, 6
- [49] Yuyang Yin, Dejie Xu, Chuangchuang Tan, Ping Liu, Yao Zhao, and Yunchao Wei. CLE diffusion: Controllable light enhancement diffusion model. In *ACMMM*, pages 8145–8156, 2023. 1, 2, 3, 4, 5
- [50] Syed Waqas Zamir, Aditya Arora, Salman Hameed Khan, Hayat Munawar, Fahad Shahbaz Khan, Ming-Hsuan Yang, and Ling Shao. Learning Enriched Features for Fast Image Restoration and Enhancement. *TPAMI*, 2022. 2, 6
- [51] Richard Zhang, Phillip Isola, Alexei A Efros, Eli Shechtman, and Oliver Wang. The unreasonable effectiveness of deep features as a perceptual metric. In *CVPR*, pages 586–595, 2018. 5
- [52] Yonghua Zhang, Jiawan Zhang, and Xiaojie Guo. Kindling the darkness: A practical low-light image enhancer. In *ACMMM*, pages 1632–1640, 2019. 2, 4, 6
- [53] Yonghua Zhang, Xiaojie Guo, Jiayi Ma, Wei Liu, and Jiawan Zhang. Beyond brightening low-light images. *IJCV*, 129:1013–1037, 2021. 2
- [54] Zhao Zhang, Huan Zheng, Richang Hong, Mingliang Xu, Shuicheng Yan, and Meng Wang. Deep color consistent network for low-light image enhancement. In *CVPR*, pages 1899–1908, 2022. 2
- [55] Chuanjun Zheng, Daming Shi, and Wentian Shi. Adaptive unfolding total variation network for low-light image enhancement. In *ICCV*, pages 4439–4448, 2021. 2
- [56] Shen Zheng and Gaurav Gupta. Semantic-guided zero-shot learning for low-light image/video enhancement. In *WACV*, pages 581–590, 2022. 2
- [57] Dewei Zhou, Zongxin Yang, and Yi Yang. Pyramid diffusion models for low-light image enhancement. *arXiv preprint arXiv:2305.10028*, 2023. 1, 2, 3, 4, 6, 7